

Tailoring photocatalytic performance of spin-Coated BiVO₄ via calcination time optimization under visible light

Gunawan Gunawan¹, Didik Setiyo Widodo¹, Nailis Sa'diyah¹, and Roni Adi Wijaya²

¹Department of Chemistry, Faculty of Science and Mathematics, Diponegoro University, Semarang-50271, Indonesia

²Department of Chemistry, Faculty of Mathematics and Natural Science, Universitas Negeri Jakarta, Jakarta Timur 13220, Indonesia

Abstract. Water pollution from synthetic dyes, particularly the toxic and non-biodegradable Rhodamine B (RhB), has spurred the development of efficient semiconductor-based photocatalytic technologies. Bismuth vanadate (BiVO₄), with a band gap of ~2.3–2.4 eV, is a promising visible-light-responsive photocatalyst. In this work, BiVO₄ thin films were fabricated on FTO substrates via spin coating, followed by calcination at 500 °C for varying durations (5, 10, 15, 20, and 25 min). The structural, morphological, and optical properties were characterized using XRD, SEM-EDX, UV-Vis DRS, and photoluminescence (PL) spectroscopy. Characterization confirmed the formation of monoclinic BiVO₄ with high crystallinity, a uniform surface morphology, and an optimal distribution of Bi and V elements. The optical band gap decreased from 2.30 eV (5 min) to 2.23 eV (15 min), enhancing visible-light absorption. PL spectra indicated reduced emission intensity for the 15 min sample, suggesting improved charge-separation efficiency. Photocatalytic experiments demonstrated that the 15 min calcined BiVO₄ achieved the highest photocurrent density (90 μA/cm²) and an RhB degradation efficiency of 85.96% within 100 min, following pseudo-first-order kinetics. These results highlight that spin-coated BiVO₄ thin films with optimised calcination time exhibit superior structural, optical, and photoelectrochemical properties, making them promising candidates for visible-light-driven wastewater remediation.

1 Introduction

Water contamination caused by industrial effluents containing synthetic dyes has emerged as one of the most pressing global environmental challenges [1–3]. Among these pollutants, Rhodamine B (RhB) is a highly toxic, carcinogenic, and non-biodegradable xanthene dye that poses significant risks to both aquatic ecosystems and human health due to its persistence and bioaccumulation potential. Conventional treatment methods, such as adsorption, coagulation, biological degradation, and membrane filtration, often exhibit limited efficiency and generate secondary waste. Consequently, semiconductor-based photocatalysis has garnered significant

¹ Corresponding author: gunawan@live.undip.ac.id

attention as a sustainable and cost-effective technology for degrading organic pollutants under solar or visible light irradiation [4].

Bismuth vanadate (BiVO_4) has emerged as one of the most promising visible-light-driven photocatalysts owing to its suitable band gap (2.3–2.4 eV), non-toxicity, chemical stability, and appropriate valence and conduction band positions for oxidative reactions [5]. In particular, monoclinic scheelite BiVO_4 exhibits superior photocatalytic activity compared to tetragonal or zircon-type phases, mainly due to its efficient charge transport and strong absorption in the visible region [6]. However, the photocatalytic efficiency of BiVO_4 is often limited by rapid electron–hole recombination, poor carrier mobility, and relatively low surface area. Despite these advances, optimizing synthesis and thermal treatment parameters remains a practical and straightforward approach to improving BiVO_4 performance without introducing complex fabrication steps.

Among various synthesis routes, solution-based deposition methods such as spin coating, dip coating, and sol–gel processes offer simple, scalable, and controllable fabrication of BiVO_4 thin films with tunable thickness and uniformity [7]. The post-deposition calcination step plays a crucial role in determining the crystallinity, grain size, surface morphology, and defect structure of the resulting thin films, which directly influence light absorption, charge separation, and photocatalytic activity [8]. Optimizing the calcination time is particularly important, as insufficient heating may lead to incomplete crystallization. In contrast, excessive calcination can induce grain coarsening and the annihilation of oxygen vacancies, thereby reducing the number of active surface sites. The influence of short calcination durations on the structural evolution and charge-carrier dynamics of spin-coated BiVO_4 thin films remains insufficiently explored, particularly from a photoelectrode perspective. Short calcination durations were selected to balance incomplete crystallization and over-annealing effects in BiVO_4 thin films, which are more thermally sensitive than powder photocatalysts due to their limited thickness and substrate interactions. In this work, we systematically investigate the effect of calcination time on crystallinity, recombination behaviour, and photoelectrochemical performance, providing a practical thermal optimization strategy for BiVO_4 thin-film photoanodes.

In this study, BiVO_4 thin films were synthesized on fluorine-doped tin oxide (FTO) substrates via spin coating followed by calcination at 500 °C with varying durations (5–25 min). The effects of calcination time (5–25 min at 500 °C) on the structural, morphological, optical, and photoelectrochemical properties of spin-coated BiVO_4 thin films were systematically investigated. XRD, SEM-EDX, UV–Vis DRS, and PL analyses were used to elucidate crystallinity, elemental composition, optical band gap, and charge-recombination behavior. The photocatalytic performance was evaluated using RhB degradation under visible-light irradiation. The results demonstrate that an optimized calcination time of 15 min yields highly crystalline monoclinic BiVO_4 with improved charge separation efficiency and enhanced photocurrent response, resulting in superior photocatalytic degradation efficiency. This study provides new insights into the correlation among calcination time, structural evolution, and the photocatalytic activity of spin-coated BiVO_4 thin films, highlighting a facile route to developing efficient photoactive materials for visible-light-driven wastewater remediation.

2 Experimental

2.1 Materials and instruments

The materials used include bismuth nitrate pentahydrate ($\text{Bi}(\text{NO}_3)_3 \cdot 5\text{H}_2\text{O}$), vanadyl acetylacetonate ($\text{VO}(\text{acac})_2$), acetylacetone, acetic acid, sodium sulfate (Na_2SO_4), disodium hydrogen phosphate dihydrate ($\text{Na}_2\text{HPO}_4 \cdot 2\text{H}_2\text{O}$), sodium hydroxide (NaOH), ethanol, acetone, deionized water, aquadest, Fluorine-doped tin oxide (FTO) glass, Rhodamine B (RhB),

terephthalic acid ($C_6H_4(CO_2H)_2$, Merck), 2-hydroxyterephthalic acid (HTA, Merck), and deionized water, and high-purity nitrogen gas were used throughout the experiments. All reagents were used as precursor chemicals without further purification. The instruments used include general laboratory glassware (Herma), analytical balance (Ohaus, Model PA323), pH meter, hot plate with a magnetic stirrer (Faithful), furnace (Thermo Scientific), sonicator (Taffware, Model GA008), desiccator, asahi solar simulator (15 W, Krisbow, Model FTC451) equipped with light chopper and monochromator, potentiostat (CorrTest CS Studio 150) with three electrode system (platinum counter, Ag/AgCl reference, and substrate as working electrode), a spin coater for thin film deposition, an FTC45115 Watt UV lamp as the visible-light irradiation source, X-ray diffractometer (XRD, D8 Advance Bruker, Bragg-Brentano configuration), scanning electron microscope (SEM, JSM-6510LA), energy dispersive X-ray spectrometer (EDS, ISIS 300, Oxford, UK), UV-VIS-NIR spectrophotometer (Shimadzu, UV-2450 Plus), fluorescence spectrophotometer (Cary Eclipse MY19350001), and UV-Vis spectrophotometer (Shimadzu, UV-1280).

2.2 Preparation of $BiVO_4$ spin-coated thin film

A $BiVO_4$ thin film was prepared by spin coating. FTO substrates were sequentially ultrasonically cleaned in acetone, ethanol, and deionized water for 15 min each, then dried under ambient conditions. The substrates were then dried under ambient conditions before film deposition. The precursor solution was prepared by dissolving 0.297 g of $Bi(NO_3)_3 \cdot 5H_2O$ in 3 mL of glacial acetic acid and 0.1624 g of $VO(acac)_2$ in 15 mL of acetylacetone. Both solutions were stirred separately until completely homogeneous, then mixed under continuous stirring. The resulting mixed precursor solution was further sonicated for 30 min to ensure uniformity and stability. The $BiVO_4$ thin films were fabricated by spin-coating a precursor solution (3-5 drops from a pipette) onto cleaned FTO substrates at 500 rpm and an acceleration of 3000 rpm/s for 30 s, followed by preheating at 150 °C for 5 min to remove residual solvents and promote adhesion. This process was repeated several times over 6 coating cycles. Finally, the spin-coated films were calcined at 500 °C for 5, 10, 15, 20, and 25 minutes in ambient air. This thermal treatment was performed to induce crystallization of $BiVO_4$ and to optimize the thin films' microstructural and optical properties.

2.3 Characterization of thin film

The obtained thin films were subjected to comprehensive characterization. The surface morphology and elemental composition were examined using a scanning electron microscope (SEM, JSM-6510LA) coupled with an energy-dispersive X-ray spectrometer (EDS, ISIS 300, Oxford, UK). Crystalline phases and structural properties were determined by X-ray diffraction (XRD; Bruker D8 Advance, $Cu K\alpha$ radiation with a Ni filter). Optical absorption spectra were recorded using a UV-Vis-NIR spectrophotometer (Shimadzu UV-2450 Plus) to estimate the band gap energy. Photoluminescence (PL) spectra were obtained using a Cary Eclipse fluorescence spectrophotometer to evaluate the recombination behavior of photogenerated charge carriers.

2.4 Photoelectrochemical measurements

Photoelectrochemical (PEC) measurements were performed using a CorrTest CS-150 potentiostat/galvanostat equipped with a 0.1 mHz–2 MHz digital function generator (DF 1906, NF Japan, 0.3 Hz) and a Shutter Controller F77 (Suruga Seiki). Linear sweep voltammetry (LSV) was recorded under an Asahi Solar Simulator (15 W, Krisbow, Model FTC451) at a scan rate of 10 mV s⁻¹, with a range of 1.2–0 V vs Ag/AgCl for $BiVO_4$. A 0.1 M Na_2SO_3 aqueous solution

was used as the electrolyte, employing a three-electrode configuration with BiVO₄ thin films as the working electrode, a Pt as the counter electrode, and an Ag/AgCl reference electrode.

2.5 Application as a photocatalyst for RhB degradation

Photoelectrochemical (PEC) measurements were performed in a three-electrode configuration, using the fabricated BiVO₄ thin films as the working electrode, a Pt wire as the counter electrode, and an Ag/AgCl reference electrode. The experiments were carried out under visible-light irradiation provided by a 15 W solar simulator positioned 20 cm from the cell. The effects of key operational parameters, including irradiation time (0–120 min), applied potential (0–1.0 V), light illumination, and electrode sample, were systematically investigated. Dye degradation was quantified using a calibrated RhB standard curve. The degradation efficiency (η , %) was determined by monitoring the change in absorbance at the characteristic maximum wavelength (λ_{\max}) of RhB using a UV–Vis spectrophotometer over the range 200–800 nm. It was calculated according to Equation (1).

$$\text{Degradation efficiency (\%)} = [(C_0 - C_t) / C_0] \times 100\% \quad (1)$$

Where C_0 is the initial concentration, and C_t is the concentration at irradiation time t .

2.6 Kinetics and mechanism of RhB degradation

The photocatalytic kinetics of RhB dye degradation were investigated using a 30 mL aqueous solution containing 0.1 M Na₂SO₄ and RhB at an initial concentration of 20 mg/L. Absorbance changes were monitored over 0–100 min. Aliquots of 1–2 mL of the solution were collected at 20-minute intervals, and the absorbance was measured at 554–557 nm using a Shimadzu UV-2600 UV–visible spectrophotometer. The degradation of dyes was analysed using pseudo-first-order (Eqn. 2) and pseudo-second-order (Eqn. 3) kinetic models, with removal efficiency quantified by Eqn. (4).

$$\ln [C_t] = \ln [C_0] - kt \quad (2)$$

$$[1/C_t] - [1/C_0] = kt \quad (3)$$

$$\eta = (C_0 - C_t) / C_0 \times 100\% \quad (4)$$

Where C_0 and C_t are the dye concentrations (mg/L) at time 0 and t , respectively, and k is the rate constant. Kinetic parameters were determined by linear regression analysis of the experimental data.

The photodegradation mechanism was confirmed by identifying radical species in a three-electrode photoelectrochemical system. The detection of •OH radicals via the TA–HTA method confirms the generation of highly oxidative species responsible for RhB degradation under visible-light irradiation. BiVO₄ thin film as working electrode was immersed in 50 mL aqueous solution containing 0.05×10^{-3} M terephthalic acid (TA) and 0.2×10^{-3} M NaOH. An external bias of 1.0 V vs Ag/AgCl was applied under visible light illumination. During PEC operation, samples were collected at selected irradiation times (20–120 min) and analyzed with a Cary Eclipse fluorescence spectrophotometer to detect the fluorescence signal of 2-hydroxyterephthalic acid (2-HTA), characterized by an emission peak at 425 nm under 315 nm excitation [9]. The results were then calculated using the HTA, which was calibrated to the standard.

3 Results and discussions

3.1 Synthesis and Characterization of BiVO₄ Thin Films

BiVO₄ thin films were successfully synthesized on FTO substrates via a spin-coating process followed by thermal treatment, as illustrated in Figure 1. The synthesis involved three main stages: (i) precursor dissolution, (ii) intermediate phase formation through pre-heating, and (iii) crystallization during high-temperature calcination.

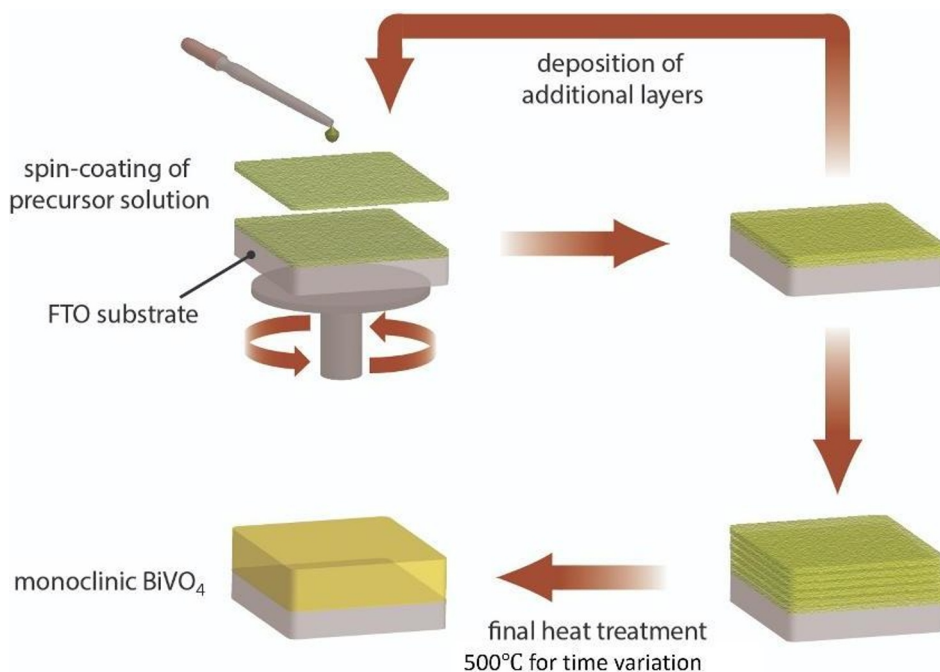
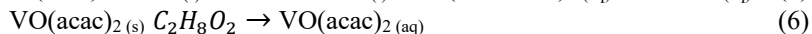
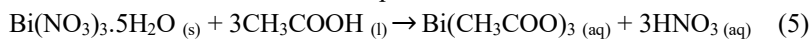


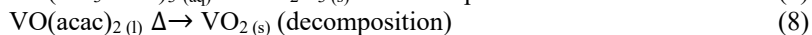
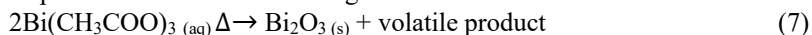
Fig. 1. Mechanism of the BiVO₄ spin coating method preparation.

In the initial step, bismuth nitrate pentahydrate (Bi(NO₃)₃·5H₂O) was dissolved in acetic acid to form bismuth acetate (Bi(CH₃COO)₃), while vanadyl acetylacetonate (VO(acac)₂) was dissolved in acetylacetonone, as described in reactions (5) and (6). Acetic acid acted as both a solvent and a complexing agent, stabilizing Bi³⁺ ions through chelation, while acetylacetonone provided a stable coordination environment for the vanadium precursor. Using acetylacetonone as a solvent contributed to the uniform distribution of the Bi and V precursors, thereby enhancing the homogeneity of the resulting thin film. After preparing a homogeneous precursor solution, the film was deposited onto the FTO substrate by spin coating, yielding uniform, thin layers. The samples were subsequently heated at 150 °C for 5 minutes, during which partial decomposition and volatilization of the organic components occurred. This pre-heating step promoted the formation of intermediate oxide phases such as Bi₂O₃ and VO₂, as shown in reactions (7) and (8). These intermediate phases played a crucial role as reactive precursors for the subsequent crystallization step. Upon calcination at 500 °C, VO₂ was oxidized to V₂O₅, which subsequently reacted with Bi₂O₃ to form the final monoclinic BiVO₄ phase according to reactions (9) and (10). The resulting thin film exhibits enhanced crystallinity and adhesion, which are crucial for achieving optimal photoelectrochemical performance.

Reaction of bismuth and vanadate precursor dissolution:



Deposition reaction with heating at 150°C:



Reaction at 500°C annealing:



The photoelectrochemical performance of the BiVO₄ thin films was evaluated through linear sweep voltammetry (LSV) under visible-light illumination, as shown in Figure 5a and Table 1. The photocurrent density significantly varied with calcination duration, reflecting the influence of crystallinity, defect density, and charge carrier transport on photoactivity [10]. The BiVO₄ film calcined for 15 min exhibited the highest photocurrent density of 90 μA/cm², compared to 58, 65, 70, and 56 μA/cm² for the films calcined at 5, 10, 20, and 25 min, respectively. This enhancement at 15 min can be attributed to the formation of a well-crystallized monoclinic BiVO₄ phase with an optimal grain size and improved interfacial contact with the FTO substrate. The improved crystallinity reduces structural disorder and enhances the migration of photogenerated charge carriers from the bulk to the surface, thereby suppressing recombination losses. In contrast, the lower photocurrent observed at shorter calcination times (5 and 10 min) is likely due to incomplete crystallization and higher defect concentrations that act as recombination centers. Prolonged calcination beyond the optimal duration (20–25 min) may induce grain coarsening and partial sintering, thereby decreasing the effective surface area and limiting the number of active reaction sites, which leads to a decline in photocurrent density.

Table 1. Photocurrent of BiVO₄ thin film by time spin coating variation.

Sample	Photocurrent (μA/cm ²)
BiVO ₄ -5 min	58
BiVO ₄ -10 min	65
BiVO ₄ -15 min	90
BiVO ₄ -20 min	70
BiVO ₄ -25 min	56

Photoluminescence (PL) spectroscopy was employed to evaluate the recombination behavior of photogenerated electron–hole pairs (**Figure 5b**). The PL spectra of BiVO₄ films calcined at 5 min and 15 min exhibit emission peaks centered around 550 nm, corresponding to band-to-band recombination transitions [11]. The BiVO₄-15 min sample shows significantly lower PL intensity than BiVO₄-5 min, indicating more efficient separation of photoexcited carriers. A lower PL emission intensity correlates with reduced radiative recombination and enhanced charge transport across the film interface, which is consistent with the observed increase in photocurrent density [12]. The suppressed recombination suggests that 15 min of optimized calcination promotes defect healing and improves crystallinity, both of which facilitate longer carrier lifetimes and better photoelectrochemical performance.

The optical absorption and band gap energies of BiVO₄ thin films were analyzed using UV–Vis diffuse reflectance spectroscopy (UV–Vis DRS), as illustrated in **Figures 5c and 5d**. The Tauc plots derived from the absorption spectra reveal direct band gap energies of **2.30 eV** for the 5-minute-prepared BiVO₄ film and 2.23 eV for the 15-minute-prepared film. The slight narrowing of the band gap with increasing calcination time can be attributed to improved lattice ordering and reduced structural distortion, which enhance electronic delocalization within the Bi–

O–V framework. This redshift in the absorption edge indicates enhanced visible-light absorption, enabling greater use of the solar spectrum for photocatalytic and photoelectrochemical applications. These enhancements are crucial for maximizing the visible-light-driven photocatalytic activity of BiVO₄ thin films, demonstrating that precise thermal control during post-deposition treatment is pivotal for tailoring the material's photoelectrochemical performance.

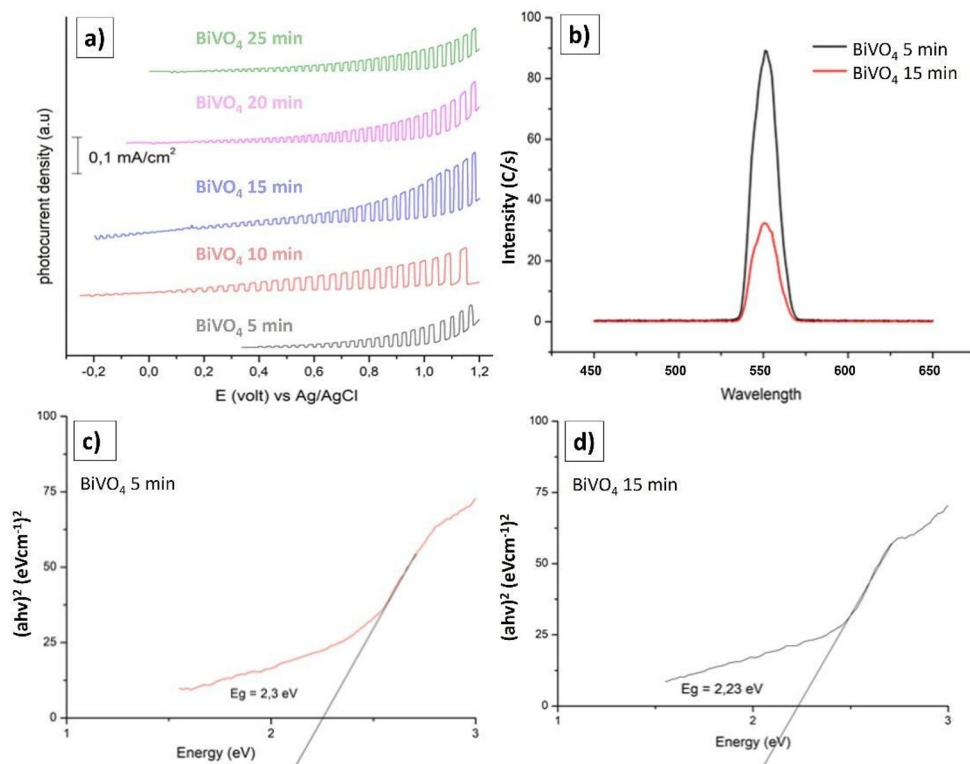


Fig. 2. Photocurrent of all-time variation time sample deposition (a); PL illumination comparison (b), and Band gap from DRS-UV Vis (c,d) of optimum (BiVO₄-15 min) and minimum (BiVO₄-5 min) deposition time of the BiVO₄ spin-coated thin film.

XRD patterns confirmed the formation of monoclinic scheelite BiVO₄ for thin films synthesized with different calcination durations (5 and 15 minutes), with no detectable impurity phases as presented in Figure (a) and Table 2. Both diffraction patterns exhibit characteristic peaks at 2θ values of approximately 19.08°, 26.67°, 29.09°, 33.87°, and 51.69°, corresponding to the (111), (110), (221), (011), and (121) planes of monoclinic scheelite BiVO₄ (JCPDS No. 14-0688), respectively [11,13]. The absence of impurity peaks related to other bismuth or vanadium oxides indicates that a pure BiVO₄ phase was successfully formed on the FTO substrate (JCPDS No. 77-0447). The 15-minute film exhibited sharper, more intense diffraction peaks than the 5-minute sample, indicating higher crystallinity and better structural order, likely due to increased film thickness and more complete grain coalescence during thermal treatment at 500 °C.

Crystallite size was estimated using the Debye–Scherrer Equation based on the prominent diffraction peaks, as summarized in Table 2. The calculated average crystallite sizes for the BiVO₄ films deposited at 5 min and 15 min were 51.12 nm and 49.10 nm, respectively. The slightly smaller crystallite size observed in the 15 min sample may result from denser, more uniform grains that limit excessive grain growth during calcination. Although both samples

exhibit nanocrystalline characteristics, the combination of sharper peaks and smaller crystallite size in the 15-minute film suggests an increased nucleation density and a more compact lattice arrangement, both of which are beneficial for charge transport and photodegradation stability.

Table 2. Crystallite size of BiVO₄ thin films.

Sample	2θ (°)	Miller index (h k l)	Diameter (nm)
BiVO ₄ -5 min	19.08	1 1 1	41.03
	26.668	1 1 0	54.98
	29.09	2 2 1	48.80
	33.872	0 1 1	54.98
	51.69	1 2 1	51.49
Average			51.12
BiVO ₄ -15 min	19.061	1 1 1	38.53
	26.668	1 1 0	55.11
	29.09	2 2 1	45.97
	33.872	0 1 1	52.94
	51.69	1 2 1	52.70
Average			49.10

The surface morphologies of the films, displayed in Figure (b), further support the structural findings. The BiVO₄ film prepared with a 5-minute calcination time exhibits a relatively smooth and featureless surface, with fine particles distributed uniformly, indicating a thin layer with limited precursor deposition. In contrast, the 15-minute BiVO₄ film exhibits a more developed granular texture, with larger, well-defined particles forming interconnected domains. This morphological evolution is associated with increased viscosity and volume of the precursor layer at longer coating durations, promoting uniform nucleation and grain growth upon calcination. The rougher and more porous surface morphology of the 15-minute sample increases the active surface area, which is advantageous for interfacial charge transfer during photocatalytic or photoelectrochemical reactions.

The elemental composition analyzed by energy-dispersive X-ray spectroscopy (EDX), shown in Figures (c) and (d), confirms the successful incorporation of bismuth, vanadium, and oxygen as the main components of BiVO₄ thin films. Minor peaks corresponding to Sn and Si are attributed to the FTO substrate and glass support, respectively. The atomic ratio of Bi to V was approximately 1:1 in both samples, consistent with the stoichiometry of BiVO₄. The 15-minute film exhibited slightly higher oxygen content and a more homogeneous elemental distribution, suggesting more complete oxidation of the precursor species and a well-formed oxide network. These results are consistent with the improved crystallinity observed in the XRD analysis. Overall, the combination of XRD, SEM, and EDX analyses demonstrates that increasing the calcination duration from 5 to 15 minutes effectively enhances the crystallinity, stoichiometric composition, and surface morphology of BiVO₄ thin films. The denser structure, improved oxygen incorporation, and refined nanocrystalline domains in the 15-minute BiVO₄ film are expected to enhance charge separation efficiency and surface reaction kinetics, making it a more promising candidate for photocatalytic and photoelectrochemical applications.

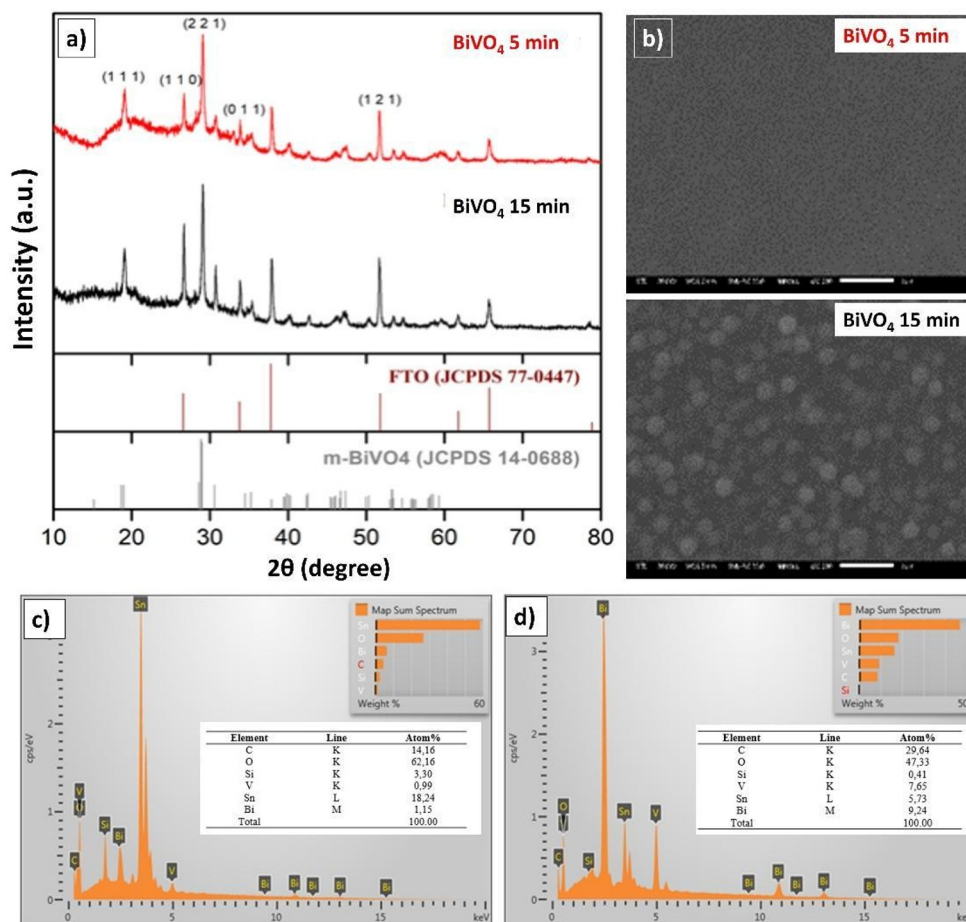


Fig. 3. XRD diffractograms (a) morphology surface (b) and Element component of BiVO₄-15 min and BiVO₄-5 min.

3.2 Photodegradation of RhB by BiVO₄ thin film

The optical calibration and photocatalytic degradation performance of a Rhodamine B (RhB) solution using a BiVO₄ thin film (15 min) as a photocatalyst were systematically investigated under visible-light irradiation. The UV-Vis absorption spectra of RhB solutions with different initial concentrations (4–20 ppm) are shown in Figure (a). All spectra exhibit a characteristic absorption peak centered at approximately 554–557 nm, corresponding to the $\pi-\pi^*$ transition of the xanthenes ring in RhB molecules. The intensity of this absorption peak increases proportionally with concentration, confirming the linear relationship between absorbance and dye concentration, as predicted by the Beer-Lambert law [14].

The calibration curve, presented in Figure (b), shows a strong linear correlation between absorbance and concentration, expressed by the regression Equation $y = 0.0438x + 0.0079$ with an excellent correlation coefficient ($R^2 = 0.9996$). This high degree of linearity demonstrates the spectrophotometric method's reliability and precision for quantitatively determining RhB concentration during the degradation process. The obtained calibration curve was subsequently used to calculate the concentration changes of RhB during visible-light irradiation in the presence of the BiVO₄ photocatalyst.

The visual changes in RhB color during the photocatalytic reaction are shown in Figure (c). The initial solution exhibits a deep pink color characteristic of RhB, which gradually fades to nearly colorless after 100 minutes of irradiation. This visual observation qualitatively confirms the progressive decomposition of RhB molecules facilitated by the BiVO₄ thin film. The quantitative degradation efficiencies, as summarized in Figure (d), further substantiate this result. The degradation efficiency increased steadily with irradiation time, achieving 56.77% at 20 minutes, 61.15% at 40 minutes, 70% at 60 minutes, 82.36% at 80 minutes, and reaching 85.96% after 100 minutes of visible-light exposure.

The remarkable photocatalytic activity of the BiVO₄ thin film (15 min) can be attributed to its optimized crystallinity, improved surface roughness, and efficient light absorption within the visible region, as previously confirmed by XRD, SEM, and UV–Vis DRS analyses. The monoclinic scheelite phase of BiVO₄ facilitates the efficient separation and transport of photogenerated charge carriers, thereby minimizing electron–hole recombination and enhancing the generation of reactive oxygen species (ROS), such as •OH and •O₂⁻ radicals. These ROS species play a crucial role in the oxidative degradation of organic dye molecules, ultimately leading to ring-opening reactions and mineralization into CO₂, H₂O, and other small inorganic ions. Overall, the calibration and degradation results demonstrate that the BiVO₄ thin film with a 15-minute spin-coating duration exhibits excellent photocatalytic efficiency for RhB degradation under visible light, confirming its potential as a stable, active photoanode material for environmental remediation and solar-driven pollutant-degradation systems.

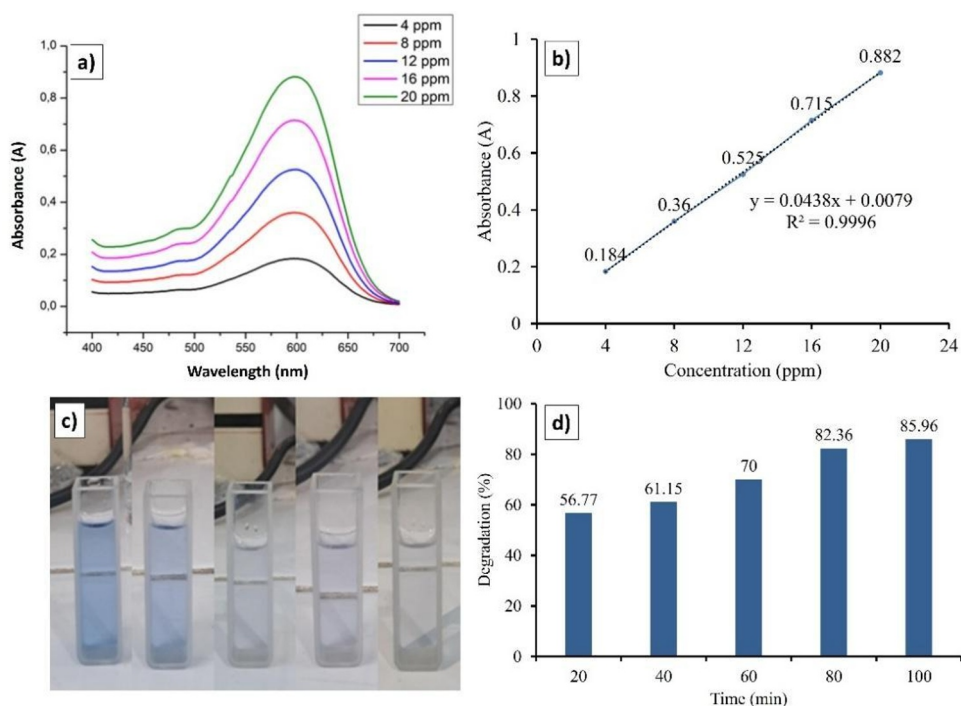


Fig. 4. Spectrum absorption of RhB by concentration variation (a), Calibration curve of RhB sample (b), visual result (c), and degradation percentage diagram (d) of RhB photodegradation by BiVO₄-15 min.

3.3 Kinetics and mechanism of RhB photodegradation

The kinetic behavior of Rhodamine B (RhB) degradation under visible light irradiation using BiVO₄ thin film (15 min calcination) was analyzed based on pseudo-first-order and pseudo-

second-order kinetic models (Figure 1a–b). The linear relationship in the pseudo-first-order plot of $\ln(C_0/C_t)$ versus time (Figure 1a) exhibited a high correlation coefficient ($R^2 = 0.953$), indicating that the photocatalytic degradation of RhB predominantly follows a pseudo-first-order kinetic model. The apparent rate constant (k) obtained from the slope was 0.0152 min^{-1} , confirming efficient degradation dynamics driven by the optimized BiVO_4 surface structure and charge-separation properties. In contrast, the pseudo-second-order plot ($1/C_t - 1/C_0$) versus time (Figure 1b) showed a slightly lower linearity ($R^2 = 0.9168$), suggesting that surface adsorption and molecular interactions play a secondary role compared to photoinduced oxidation processes. These findings demonstrate that RhB degradation is primarily governed by direct photogenerated hole- and radical-mediated oxidation rather than by chemical adsorption kinetics.

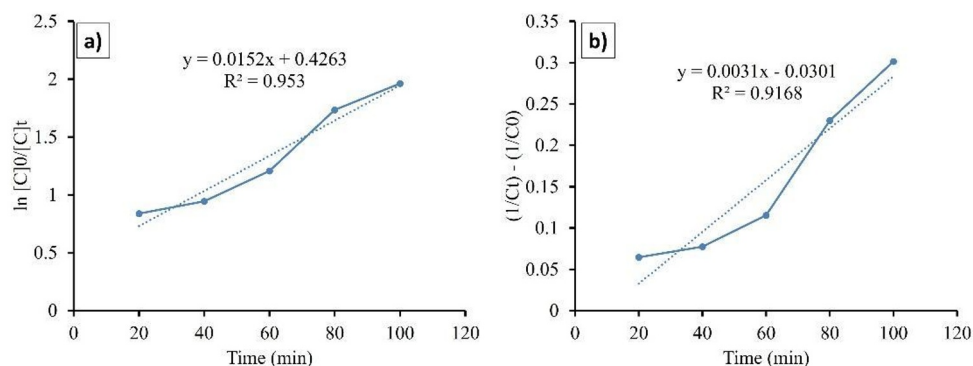


Fig. 5. Curve of pseudo-first-order and pseudo-second-order kinetic models of photodegradation of RhB by BiVO_4 -15 min.

To further elucidate the role of reactive species, particularly hydroxyl radicals ($\bullet\text{OH}$), terephthalic acid (TA) was employed as a fluorescence probe. The fluorescence spectra of 2-hydroxyterephthalic acid (HTA) formed upon reaction with $\bullet\text{OH}$ radicals showed a characteristic emission peak at 425 nm (Figure 2a). The calibration curve between HTA concentration and fluorescence intensity (Figure 2b) revealed an excellent linear relationship ($R^2 = 0.9899$), confirming the quantitative reliability of this method for $\bullet\text{OH}$ detection. The time-dependent fluorescence spectra (Figure 2c) clearly showed a gradual increase in emission intensity with prolonged irradiation, confirming the continuous generation of $\bullet\text{OH}$ radicals during photocatalysis. The reaction mechanism (Figure 2d) illustrates the conversion of TA to HTA through $\bullet\text{OH}$ attack, validating the active involvement of $\bullet\text{OH}$ in RhB degradation [9].

The quantitative analysis of $\bullet\text{OH}$ radicals at different degradation times is presented in Table 3. As the reaction time increased from 20 to 100 minutes, the fluorescence intensity of HTA rose from 95.995 to 286.158 C/s, corresponding to an increase in $\bullet\text{OH}$ radical concentration from 1.25 to 5.40 ppm. This trend shows a time-dependent increase in $\bullet\text{OH}$ generation, indicating that longer visible-light irradiation produces more reactive oxygen species due to sustained photoexcitation of BiVO_4 . The steady accumulation of $\bullet\text{OH}$ radicals indicates efficient charge-carrier separation and low recombination rates within the BiVO_4 thin film. Moreover, the substantial rise in $\bullet\text{OH}$ concentration after 80 minutes of irradiation confirms the dominance of oxidative pathways in the overall degradation mechanism, which are primarily responsible for RhB decomposition and mineralization.

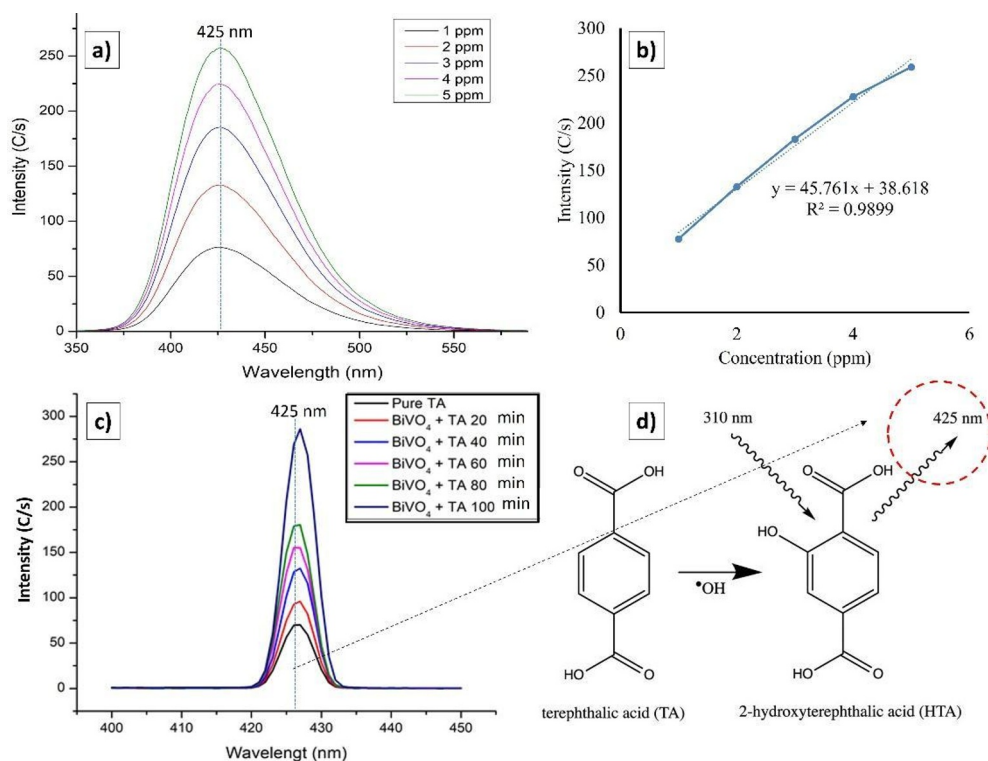


Fig. 6. PL Spectrum standard (a) and curve calibration of 2-hydroxyterephthalic acid (HTA) with concentration variation (b); PL spectrum HTA result by photodegradation RhB with BiVO_4 as radical scavenger agent by time variation (c), reaction of radical scavenger of HTA (d).

Table 3. Concentration of $\bullet\text{OH}$ radical production photodegradation by time variation.

Degradation Time (min)	Intensity of HTA (C/s)	$[\bullet\text{OH}]$ (ppm)
20	95.995	1.25
40	132.448	2.04
60	155.398	2.55
80	180.512	3.09
100	286.158	5.40

The photocatalytic degradation of Rhodamine B (RhB) over a BiVO_4 thin film prepared by spin coating proceeds via a visible-light-driven mechanism that generates photoinduced charge carriers and subsequent redox reactions at the catalyst interface. Upon visible-light irradiation, photons with energy equal to or greater than the band gap energy of BiVO_4 (≈ 2.23 eV) excite electrons from the valence band (VB) to the conduction band (CB), generating electron-hole pairs (e^-/h^+). The photogenerated holes (h^+) in the VB possess strong oxidative potential and can directly oxidize RhB molecules adsorbed on the catalyst surface. Additionally, these holes react with surface hydroxyl groups and adsorbed water molecules to generate highly reactive hydroxyl radicals ($\bullet\text{OH}$), which attack and degrade the chromophoric structures of RhB, ultimately leading to complete mineralization to CO_2 and H_2O [15].

Concurrently, the photogenerated electrons in the CB are transferred to dissolved molecular oxygen (O_2), reducing it to superoxide radicals ($\bullet\text{O}_2^-$). These reactive oxygen species participate in oxidative pathways, enhancing degradation through secondary reactions that generate

additional $\bullet\text{OH}$ and other oxidizing intermediates [6]. The synergistic activity between $\bullet\text{OH}$ and $\bullet\text{O}_2^-$ radicals results in the effective breakdown of RhB's conjugated aromatic system. Overall, the superior visible-light photocatalytic activity of the BiVO_4 thin film is primarily governed by a hydroxyl radical-dominated oxidation mechanism, supported by effective electron–hole separation and interfacial charge transfer. This indicates that the tailored BiVO_4 thin film is an efficient and stable photocatalyst for degrading organic dyes under visible-light illumination.

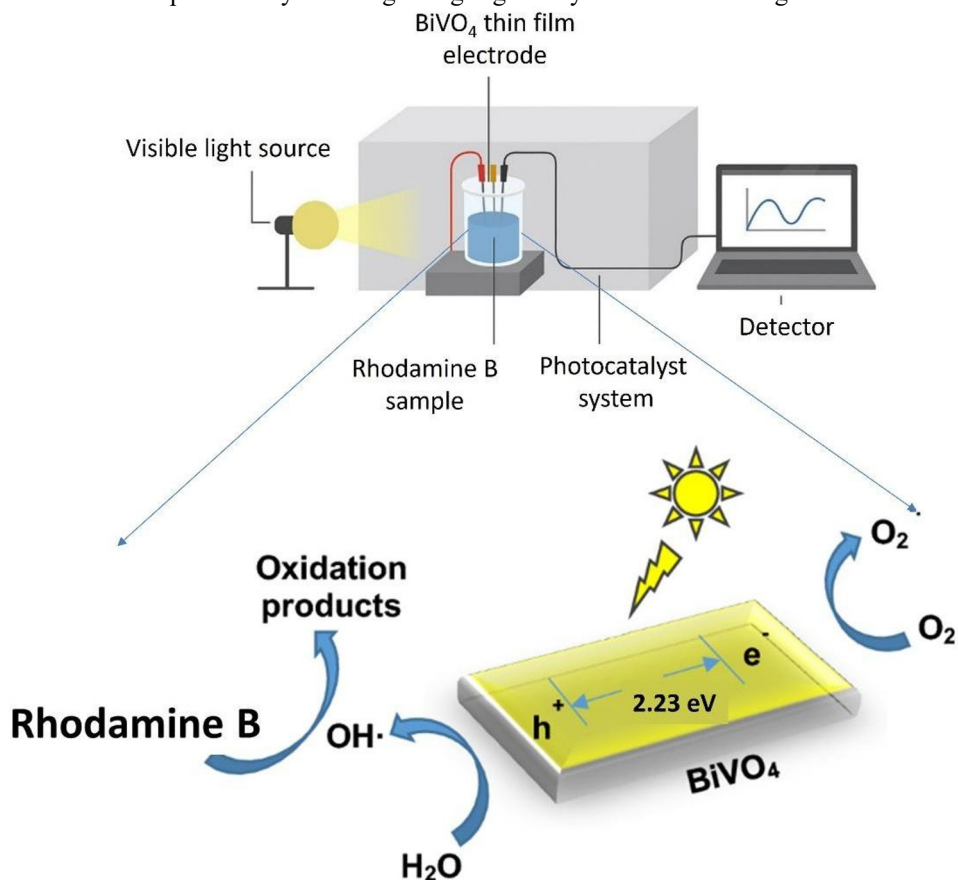


Fig. 7. Mechanism of RhB photodegradation by BiVO_4 spin-coated thin film.

4 Conclusion

Spin-coated BiVO_4 thin films were successfully fabricated on FTO substrates and thermally treated at $500\text{ }^\circ\text{C}$ with varying calcination times to elucidate the role of short-time annealing on photoelectrochemical and photocatalytic performance. All samples crystallized in the monoclinic scheelite phase, with calcination time strongly influencing crystallinity, optical absorption, and charge-carrier recombination behavior. An optimal calcination time of 15 min produced the most favorable balance between crystallinity and defect-related recombination, as evidenced by suppressed photoluminescence intensity, a narrowed band gap (2.23 eV), and the highest photocurrent density ($90\ \mu\text{A}/\text{cm}^2$). These improvements indicate enhanced charge-separation and carrier-transport efficiency in the optimized thin film. The optimized BiVO_4 thin film exhibited superior visible-light-driven photocatalytic activity toward Rhodamine B degradation, achieving 85.96% removal within 100 min and following pseudo-first-order kinetics. Radical probe experiments confirmed the dominant contribution of hydroxyl radicals ($\bullet\text{OH}$) in the degradation

process, consistent with efficient photoinduced charge separation and interfacial redox reactions. Overall, this study demonstrates that precise control of calcination time on the minute scale is an effective and practical strategy for tuning the photoactivity of BiVO₄ thin-film photoanodes. The findings provide insights into thermal optimization of spin-coated BiVO₄ thin films and support their potential application in visible-light-driven wastewater remediation.

Acknowledgement

The authors thank the World Class Research University Program, Diponegoro University (SPK No: 357-21/UN7.D2/PP/IV/2024) for sponsoring this research.

References

1. F. Gozzi, D.R.V. Guelfi, T.F. da Silva, S.C. de Oliveira, A. Machulek Junior, Recent developments on the application of photoelectrochemical processes for sustainable water treatment, *Curr. Opin. Electrochem.* **46** (2024) 101502. <https://doi.org/10.1016/J.COEELEC.2024.101502>.
2. G. Gunawan, N.B.A. Prasetya, R.A. Wijaya, W. Septina, Investigation of electrocoagulation with hydroxide-activated aluminum-copper (Al/Cu) internal micro-electrolysis system for aquaculture, dye, and antibiotic wastewater treatment, *Journal of Water Process Engineering* **71** (2025) 107155. <https://doi.org/10.1016/J.JWPE.2025.107155>.
3. G.A. Kallawar, B.A. Bhanvase, A review on existing and emerging approaches for textile wastewater treatments: challenges and future perspectives, *Environmental Science and Pollution Research* **31** (2023) 1748–1789. <https://doi.org/10.1007/S11356-023-31175-3>.
4. G. Gunawan, N.B.A. Prasetya, D.S. Widodo, R.A. Wijaya, Electrochemical Degradation of Methylene Blue With Seawater and Pb/PbO₂ Electrodes From Battery Waste, *Karbala International Journal of Modern Science* **9** (2023) 725–741. <https://doi.org/10.33640/2405-609X.3333>.
5. B. Guan, J. Chen, Z. Li, Z. Zhuang, Y. Chen, Z. Ma, J. Guo, C. Zhu, X. Hu, S. Zhao, H. Dang, L. Chen, K. Shu, Z. Guo, K. Shi, Y. Li, C. Yi, J. Hu, Z. Huang, Review on Synthesis, Modification, Morphology, and Combination of BiVO₄-based Catalysts for Photochemistry: Status, Advances, and Perspectives, *Energy & Fuels* **38** (2023) 806–853. <https://doi.org/10.1021/ACS.ENERGYFUELS.3C03932>.
6. A.Z. Ali, S. Jagannathan, Y.D. Bennani, J.P. van der Hoek, H. Spanjers, Photoelectrocatalytic based simultaneous removal of multiple organic micro-pollutants by using a visible light driven BiVO₄ photoanode, *Journal of Water Process Engineering* **56** (2023) 104471. <https://doi.org/10.1016/J.JWPE.2023.104471>.
7. J. Cai, J. Wang, F. Li, X. Zhang, B. Feng, Z. Yu, Y. Li, Preparation of BiVO₄ Films and Modulation of Their Photocatalytic Properties by Pulsed Laser Deposition, Magnetron Sputtering, and Atomic Layer Deposition, *ACS Appl. Electron. Mater.* **7** (2025) 5331–5353. <https://doi.org/10.1021/ACSAELM.5C00566>.
8. D. Caus, K. Berent, K. Mech, A. Naumov, M. Marciszko-Wiackowska, A. Podborska, Comparative Studies on Synthesis Methods of BiVO₄ for Photoelectrochemical Applications, *Molecules* **2025**, Vol. **30**, Page 3818–3830 (2025) 3818. <https://doi.org/10.3390/MOLECULES30183818>.
9. G. Gunawan, N. Basid Adiwibawa Prasetya, R. Adi Wijaya, Electrosynthesis of ferrate from iron waste and seawater salts as Antibacterials for water pollutant treatment, *Chemical Engineering Journal* **498** (2024) 155422. <https://doi.org/10.1016/J.CEJ.2024.155422>.

10. N. Thi Huyen, T.V.H. Luu, Tran Le, H. Phuc Dang, Structure–property–performance correlation in BiVO₄ photoanodes synthesized by intensity-tuned pulse electrodeposition, *Nanoscale Adv.* (2025). <https://doi.org/10.1039/D5NA00667H>.
11. P. Arunachalam, M.S. Amer, A.M. Al-Mayouf, A.A. Alsaleh, Surface Engineering of BiVO₄ Photoanodes for Photoelectrochemical Water Splitting: Recent Advances, *ChemCatChem* **16** (2024) e202400312. <https://doi.org/10.1002/CCTC.202400312>.
12. X. Li, S. Hou, X. Xie, H. Yang, Y. Huang, Lattice strain engineering via electrochemical treatment boosts solar water oxidation of BiVO₄ through accelerated intermediate conversion, *J. Catal.* **453** (2026) 116540. <https://doi.org/10.1016/J.JCAT.2025.116540>.
13. N. Thi Huyen, Thi Viet Ha Luu, T. Le ab, H. Phuc Dang, Structure–property–performance correlation in BiVO₄ photoanodes synthesized by intensity-tuned pulse electrodeposition, *Nanoscale Adv.* **7** (2025) 7182–7195. <https://doi.org/10.1039/D5NA00667H>.
14. A. Ilyas, K. Rafiq, M.Z. Abid, A. Rauf, E. Hussain, Growth of villi-microstructured bismuth vanadate (Vm-BiVO₄) for photocatalytic degradation of crystal violet dye, *RSC Adv.* **13** (2023) 2379–2391. <https://doi.org/10.1039/D2RA07070G>.
15. A. Haleem, M. Ullah, S. ur Rehman, A. Shah, M. Farooq, T. Saeed, I. Ullah, H. Li, In-Depth Photocatalytic Degradation Mechanism of the Extensively Used Dyes Malachite Green, Methylene Blue, Congo Red, and Rhodamine B via Covalent Organic Framework-Based Photocatalysts, *Water* **16**, Page 1588–16 (2024) 1588. <https://doi.org/10.3390/W16111588>.